

Colloidal Synthesis of Cu_2SnSe_3 Tetrapod Nanocrystals

Jianjun Wang, Ajay Singh, Pai Liu, Shalini Singh, Claudia Coughlan, Yina Guo, and Kevin M Ryan*

Materials and Surface Science Institute (MSSI) and Department of Chemical and Environmental Sciences, University of Limerick, Limerick, Ireland

S Supporting Information

ABSTRACT: The formation of Cu_2SnSe_3 tetrapod nanocrystals is reported using a hot injection colloidal synthesis. The ternary copper chalcogenide nanocrystals nucleate with a cubic core with four short wurtzite arms.

In colloidal semiconductor nanocrystals, significant progress in both shape and size control has allowed for targeted applications that harness their associated physical properties.¹ Each additional dimension while increasing the complexity of the nanostructure also allows for more synthetically tunable features.^{2,3} Therefore as the shape evolves from dots (0D) to rods (1D) to tetrapods (3D), properties such as total conductivity, photon absorption, etc. can be manipulated according to arm length and diameter.^{4,5} The spatial distribution of the vertices can also aid the final device with tetrapods functioning as single electron transistors with the core always addressable by three supporting arms at the substrate.^{6,7} Similarly in hybrid nanocrystal polymer photovoltaics, the branched shape maximizes the number of sites for exciton separation while allowing for directed electron pathways.⁸ Their three-dimensional construct also makes tetrapods of interest in engineering materials not only as a strengthening additive but also for strain detection where the stress on the arms changes the optoelectronic properties.² Significant progress in understanding assembly has allowed extension to superstructure formation over practical length scales.^{9,10}

Many possible mechanisms can induce the formation of branched nanocrystals in solution with polymorphism the critical enabler.² In tetrapods, first nucleation occurs in the cubic sphalerite phase with four {111} facets with subsequent growth of the hexagonal wurtzite phase from each facet along the [001] direction.^{5,6,11} Precise conditions are needed to switch from nucleation in the cubic phase to growth in the wurtzite phase. A key parameter for achieving tetrapod growth is the energy difference between the wurtzite and the cubic structures, which is mainly determined by temperature in addition to the type, functionality, and concentration of ligand molecules.^{12–15} The first tetrapods were observed in the well studied cadmium chalcogenide system.^{2–6} Extension to other semiconductors has remained elusive, although there have been reports with hydrothermally grown wide band gap oxides (ZnO).⁷ Recently, colloidal hot-injection routes to copper chalcogenide based nanocrystals have attracted a lot of interest.^{12–16} These materials are well-known for the importance in thin-film photovoltaics, and their formation as nanocrystals has allowed for solution processed devices with

high efficiencies.^{15,17,18} A further advantage is that the inclusion of additional transition metals, e.g. Sn, allows for tuning of the band gap over a specific range while benefiting from the high earth abundance of key elements.^{19–21} Cu_2SnSe_3 (CTSe) in particular has a band gap ranging from 0.8 to 1.7 eV, a high optical absorption coefficient ($\sim 10^4$ – 10^5 cm^{-1}) and relatively high hole mobilities.^{19,22–24} Recently, colloidal CTSe nanocrystals and their quaternary analogues have been reported in both the cubic and wurtzite structures.^{13,19,22,23,25} The wurtzite phase in copper chalcogenides is metastable only occurring in nanocrystals and not in the bulk.^{12–16,21} Most reported syntheses have reported either one or the other phase although polytopic crystals with both phases have been observed in 0D or 1D structures.^{26,27} Here, we report the synthesis of Cu_2SnSe_3 as 3D tetrapods showing the attainability of more complex structures in these systems.

In a typical process, CuCl (0.250 mmol), SnCl_2 (0.125 mmol), and 10 mL oleylamine were added in a three-neck flask and evacuated at 60 °C for 20 min. The solution was then heated to 310 °C under an argon atmosphere. At the same time, diphenyl diselenide (0.188 mmol) was mixed with 2 mL of oleylamine in another flask and evacuated at room temperature for 30 min. At 310 °C, the diphenyl diselenide solution was injected into the metal solution by syringe, resulting in an immediate color change from light yellow to black. After injection, the temperature drops to 295–300 °C and the reaction was allowed to proceed at that temperature for 15 min with continuous stirring. The reaction was terminated by removal of the heating mantle and allowed to cool to room temperature naturally. The product was washed using a typical procedure, and larger nanocrystals and aggregates were removed on centrifugation (see Supporting Information for additional experimental details). The final tetrapod nanocrystals were dispersed in toluene for further characterization.

Transmission electron microscopy (TEM), and dark field TEM, Figure 1a, b, demonstrated that the nanocrystals are constructed by one core and four arms distributed symmetrically. As reported for Cd-based tetrapods, the fourth arm overlaps with the core, making the contrast more profound.^{3,5,6} The large area TEM image (Figure 1c) indicates that the as-synthesized NCs are well dispersed with an average arm diameter of 28.2 nm and a length of 17.5 nm. The selected-area electron diffraction (SAED) pattern (inset of Figure 1c) can be indexed with rings corresponding to the presence of both cubic and wurtzite phases of CTSe confirming the expected structure.

Received: March 27, 2013

Published: May 10, 2013

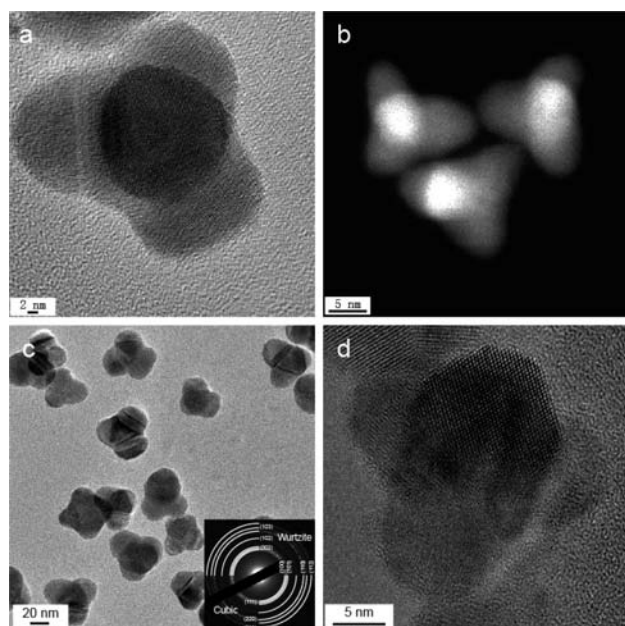


Figure 1. (a) TEM image of a CTSe tetrapod. (b) Dark field TEM image of tetrapods. (c) CTSe tetrapods with an average arm diameter of 28.2 nm and length of 17.5 nm (inset SAED pattern indexed to cubic and wurtzite phases). (d) Further TEM image of a tetrapod at angular offset.

Tilting the sample can bring the fourth arm into view as shown in Figure 1d.

Figure 2 shows HRTEM images of an individual CTSe tetrapod with four zones indicated in each comprising the core and the three in-plane arms. The lattice fringing confirms the crystallinity of the tetrapods, and the FFT of each zone was used to calculate the lattice spacing and reveal the texture. Due to the viewing angle, the observed d -spacing and the angle between two planes slightly deviate from the theoretical values. The observed d -spacings (about 0.34 and 0.33 nm) correspond to the (111) and (002) planes of cubic CTSe, respectively. The angles between the observed planes are 57° and 66° , slightly offset from theoretical values of 55° and 71° .²⁶ The lattice fringing (~ 0.20 nm) from the CTSe tetrapod arm structure occurs predominantly from the (110) planes due to the angular offset from the normal due to their tetrahedral geometry. This is typically not observed in longer arm cadmium chalcogenide tetrapods, as during drying the capillary forces pull the arms flat. The arms were epitaxially grown from the four $\langle 111 \rangle$ directions of the cubic cores, as shown in Figure 2b, c. The difference in lattice fringing from the arm labeled II to that of arms III and IV is due to the different viewing direction. For arm II, the lattice fringing extends from the (220) plane of the cubic core to the (110) plane of the wurtzite arm perpendicular to the interface, while, for arms III and IV, the lattice finger extends from the (220) plane of the cubic core to the (013) plane of the wurtzite arm with an angle of 30° to the interface. The observations agree with the crystal model confirming the direction of growth for all arms is $[001]$. For some tetrapods with a longer arm, lattice fringing from the (002) planes dominates as expected (from flattening of the arm in plane (Figure S6), further confirming the $[001]$ growth direction).

Energy dispersive X-ray spectroscopy was utilized to measure the composition of as-synthesized tetrapods. Measurement of more than five randomly selected areas gave an average

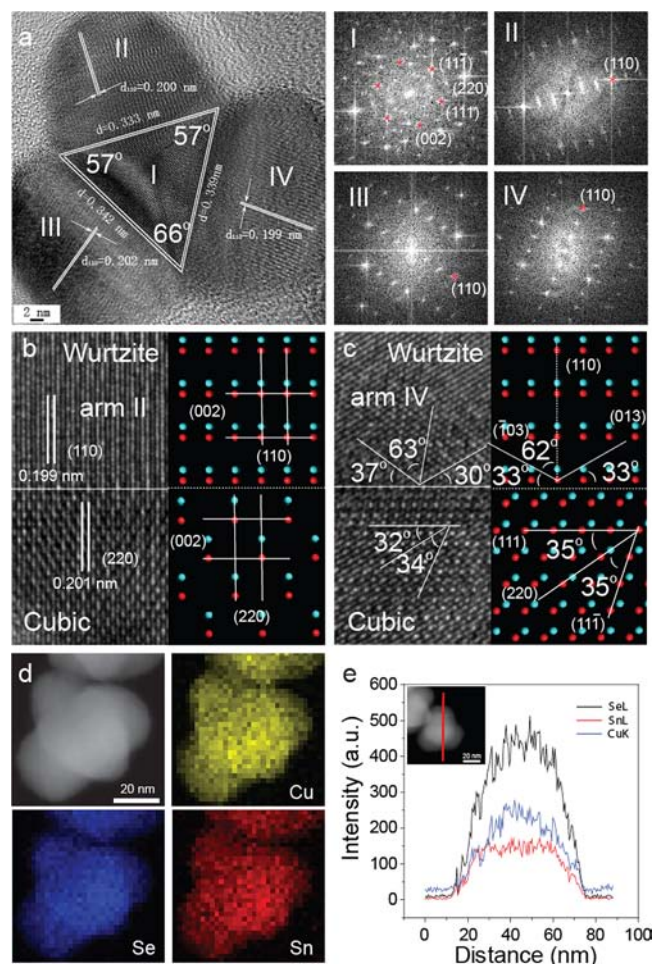


Figure 2. (a) HRTEM images of a CTSe tetrapod with their corresponding fast Fourier transform (FFT). (b) HRTEM image of interface between arm II and the core (left) and the crystal model of the interface (right). (c) HRTEM image of interface between arm IV and the core (left) and the crystal model of the interface (right). (d) STEM image and STEM-EDS elemental mappings of one CTSe tetrapod. (e) STEM-EDS line scan of one single CTSe tetrapod; the inset is the corresponding STEM image.

composition of Cu:Sn:Se = 1.82:1.00:2.94 (Table S3 and Figure S7). The tetrapods are slightly tin- and selenium-rich (Cu/Sn = 1.82; Se/(Cu + Sn) = 1.04). To further confirm the element distribution of the as-synthesized CTSe tetrapods, STEM-EDS elemental maps and the line scan were recorded, Figure 2d, e, revealing the homogeneous distribution of all three elements.

The structure of the as-synthesized NCs was characterized by X-ray diffraction (XRD), as shown in Figure 3a. Ten peaks were observed in the present measuring range. The main peaks at 25.6° , 27.1° , 28.9° , 37.4° , 45.1° , 48.7° , and 53.4° could be indexed to the (100), (002), (101), (102), (110), (103), and (112) planes of the wurtzite structure. As the (111), (220), and (311) planes of the cubic-CTSe overlap with the (002), (110), and (112) planes of WZ-CTSe, the stronger diffraction of those peaks than expected coupled with the peak at 65.5° , characteristic of the (400) plane of the cubic structure, confirms both phases. The lattice parameter was calculated from the experimental XRD pattern by fitting the main diffraction peaks corresponding to the cubic and wurtzite structures. The lattice parameters of the hexagonal structure are

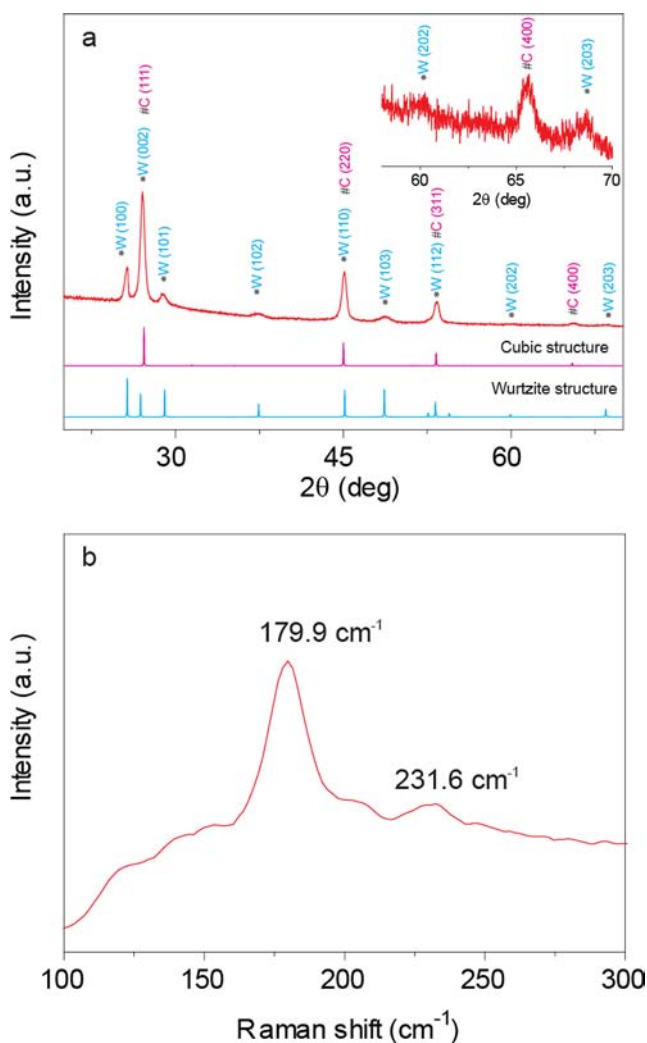


Figure 3. (a) XRD pattern of CTSe tetrapods and simulated XRD pattern of cubic and wurtzite structures. (b) Raman spectra of CTSe product.

$a = b = 4.0146 \text{ \AA}$ and $c = 6.6482 \text{ \AA}$, which agree well with those that have been reported previously.^{13,19} The lattice parameter calculated for the cubic structure is $a = 5.6922 \text{ \AA}$ by fitting the (400) reflection, which is consistent with the JCPDS database (no. 65-7524). These lattice parameters were used to simulate the XRD pattern of the cubic and wurtzite structure CTSe. The structure can be derived from ZnSe by randomly substituting Zn ions with Cu and Sn ions. Cu and Sn ions share the same position, and their occupancy possibilities are 2/3 and 1/3, respectively.^{13,15,16,19} The simulated XRD patterns are shown in Figure 3a.

Given that binary compounds such as Cu_2Se have an XRD pattern that overlaps with that of CTSe, Raman spectra were further used to confirm the structure of the product. In the typical Raman spectra of the sample as shown in Figure 3b, two obvious peaks were observed. The Raman shift for the stronger peak observed at 179.9 cm^{-1} can be assigned to the main mode of CTSe and originates from the motion between the Se atom and Cu atom as well as the Sn atom at rest.^{28,29} The other peak observed at 231.6 cm^{-1} matches well with the previous reports.²⁸ The absence of peaks around 260 cm^{-1} , corresponding to CuSe or Cu_2Se , and peaks around 150 and 110 cm^{-1}

corresponding to SnSe or SnSe_2 confirmed the purity of the CTSe phase without any additional binary compounds.^{30,31}

The optical properties were investigated by UV-vis-NIR absorption spectroscopy (Figure 4). The as-synthesized tetrapods have a significant absorption in the UV to visible spectral region. The optical band gap was estimated by using a method based on the relation of $(\alpha h\nu)^2$ versus $h\nu$ (where α is absorbance, h is Planck's constant, and ν is frequency). The result demonstrates an effective optical band gap of $\sim 1.34 \text{ eV}$, which is higher than that of thin films ($0.8\text{--}1.1 \text{ eV}$) and moderate for solution processed nanocrystals ($0.9\text{--}1.7 \text{ eV}$).^{13,19,22–24,29}

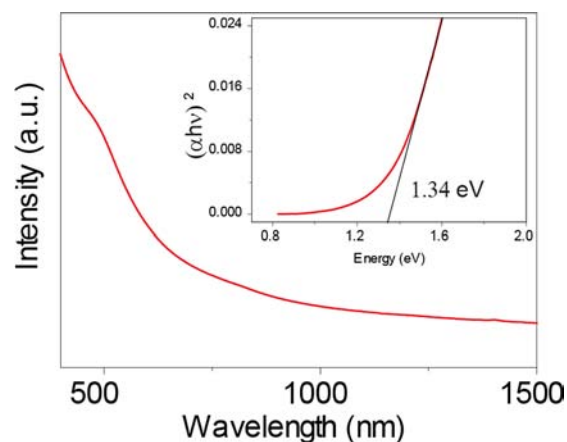


Figure 4. UV-vis-NIR absorption spectrum of CTSe tetrapods.

The synthetic protocol clearly leads to the preferential nucleation of the nanocrystals in the cubic phase with a low energy transition to growth of the metastable wurtzite arms. The critical elements of the synthesis are the initial high temperature injection ($310 \text{ }^\circ\text{C}$) that favors nucleation in the cubic phase and subsequent growth at a slightly lower temperature ($295 \text{ }^\circ\text{C}$) favoring the hexagonal phase.²⁶ The length of the tetrapod arms here were typically always comparable to the core dimensions regardless of the growth time (Supporting Information for additional syntheses) indicating that sustained growth in the [001] direction is not facilitated. Initial attempts to elongate the arms by introduction of ligands that are known to favor this growth direction disrupted tetrapod formation, likely by impeding initial formation in the cubic phase. As in comparable tetrapod syntheses, the chemistry is very finely balanced and our future studies will investigate alternative ligands/precursors coupled with in situ analysis of nucleation to allow greater tunability of the tetrapod dimensions.

In summary, CTSe tetrapods were synthesized via a hot injection colloidal method. XRD, Raman, TEM, and energy dispersive X-ray spectroscopy confirmed the tetrapods were a highly pure CTSe phase with a cubic core and four wurtzite arms. The formation of tetrapods with ternary copper chalcogenides allows for a range of potential applications from nanoelectronics to photovoltaics that can exploit their size and shape dependent properties. The facile synthesis opens pathways for extension to other compositions of multielement copper chalcogenides where the cubic and wurtzite phases can be formed.

■ ASSOCIATED CONTENT**📄 Supporting Information**

Experimental details. More TEM, HRTEM, and dark field TEM images. Details of XRD pattern simulation. EDS details. This material is available free of charge via the Internet at <http://pubs.acs.org>.

■ AUTHOR INFORMATION**Corresponding Author**

kevin.m.ryan@ul.ie

Notes

The authors declare no competing financial interest.

■ ACKNOWLEDGMENTS

This work was supported principally by Science Foundation Ireland (SFI) under the Principal Investigator Program under Contract No. 11PI-1148 and also by the Advanced Biomimetic Materials for Solar Energy Conversion Strategic Research Cluster (Contract No. 07/SRC/B1160). This work was also conducted under the framework of the Irish Government's Programme for Research in Third Level Institutions Cycle 5, National Development Plan 2007-2013 with the assistance of the European Regional Development Fund. Funding from the Irish Research Council for Science, Engineering and Technology (IRCSET) Embark initiative is acknowledged for C.C.

■ REFERENCES

- (1) Talapin, D. V.; Lee, J.-S.; Kovalenko, M. V.; Shevchenko, E. V. *Chem. Rev.* **2010**, *110*, 389.
- (2) Li, H.; Kanaras, A. G.; Manna, L. *Acc. Chem. Res.* **2013**, DOI: 10.1021/ar3002409.
- (3) Milliron, D. J.; Hughes, S. M.; Cui, Y.; Manna, L.; Li, J.; Wang, L.-W.; Alivisatos, A. P. *Nature* **2004**, *430*, 190.
- (4) Jun, Y.-w.; Choi, J.-s.; Cheon, J. *Angew. Chem., Int. Ed.* **2006**, *45*, 3414.
- (5) Manna, L.; Milliron, D. J.; Meisel, A.; Scher, E. C.; Alivisatos, A. P. *Nat. Mater.* **2003**, *2*, 382.
- (6) Chen, M.; Xie, Y.; Lu, J.; Xiong, Y.; Zhang, S.; Qian, Y.; Liu, X. *J. Mater. Chem.* **2002**, *12*, 748.
- (7) Lupan, O.; Chow, L.; Chai, G. *Sens. Actuators, B* **2009**, *141*, 511.
- (8) Sun, B.; Marx, E.; Greenham, N. C. *Nano Lett.* **2003**, *3*, 961.
- (9) Zanella, M.; Bertoni, G.; Franchini, I. R.; Brescia, R.; Manna, L. *Chem. Commun.* **2011**, *47*, 203.
- (10) (a) Singh, A.; Coughlan, C.; Laffir, F.; Ryan, K. M. *ACS Nano* **2012**, *6*, 6977. (b) Singh, A.; Gunning, R. D.; Ahmed, S.; Barrett, C. A.; English, N. J.; Garate, J.-A.; Ryan, K. M. *J. Mater. Chem.* **2012**, *22*, 1562. (c) Kelly, D.; Singh, A.; Barrett, C. A.; O'Sullivan, C.; Coughlan, C.; Laffir, F. R.; O'Dwyer, C.; Ryan, K. M. *Nanoscale* **2011**, *3*, 4580. (d) Singh, A.; Gunning, R. D.; Sanyal, A.; Ryan, K. M. *Chem. Commun.* **2010**, *46*, 7193.
- (11) Ding, Y.; Wang, Z. L.; Sun, T.; Qiu, J. *Appl. Phys. Lett.* **2007**, *90*, 153510.
- (12) Kruszynska, M.; Borchert, H.; Parisi, J. r.; Kolny-Olesiak, J. *J. Am. Chem. Soc.* **2010**, *132*, 15976.
- (13) Norako, M. E.; Greaney, M. J.; Brutchey, R. L. *J. Am. Chem. Soc.* **2012**, *134*, 23.
- (14) Singh, A.; Geaney, H.; Laffir, F.; Ryan, K. M. *J. Am. Chem. Soc.* **2012**, *134*, 2910.
- (15) Wang, J.-J.; Hu, J.-S.; Guo, Y.-G.; Wan, L.-J. *NPG Asia Mat.* **2012**, *4*, e2.
- (16) Pan, D.; An, L.; Sun, Z.; Hou, W.; Yang, Y.; Yang, Z.; Lu, Y. *J. Am. Chem. Soc.* **2008**, *130*, 5620.
- (17) Guo, Q.; Kim, S. J.; Kar, M.; Shafarman, W. N.; Birkmire, R. W.; Stach, E. A.; Agrawal, R.; Hillhouse, H. W. *Nano Lett.* **2008**, *8*, 2982.
- (18) Guo, Q.; Ford, G. M.; Yang, W.-C.; Walker, B. C.; Stach, E. A.; Hillhouse, H. W.; Agrawal, R. *J. Am. Chem. Soc.* **2010**, *132*, 17384.

- (19) Li, S.; Pan, D. *J. Cryst. Growth* **2012**, *358*, 38.
- (20) Wang, J.-J.; Xue, D.-J.; Guo, Y.-G.; Hu, J.-S.; Wan, L.-J. *J. Am. Chem. Soc.* **2011**, *133*, 18558.
- (21) Wang, Y.-H. A.; Zhang, X.; Bao, N.; Lin, B.; Gupta, A. *J. Am. Chem. Soc.* **2011**, *133*, 11072.
- (22) Ibáñez, M.; Cadavid, D.; Anselmi-Tamburini, U.; Zamani, R.; Gorsse, S.; Li, W.; López, A. M.; Morante, J. R.; Arbiol, J.; Cabot, A. *J. Mater. Chem. A* **2013**, *1*, 1421.
- (23) Ahmadi, M.; Pramana, S. S.; Batabyal, S. K.; Boothroyd, C.; Mhaisalkar, S. G.; Lam, Y. M. *Inorg. Chem.* **2013**, *52*, 1722.
- (24) Kuo, D.-H.; Haung, W.-D.; Huang, Y.-S.; Wu, J.-D.; Lin, Y.-J. *Thin Solid Films* **2010**, *518*, 7218.
- (25) Coughlan, C.; Singh, A.; Ryan, K. M. *Chem. Mater.* **2013**, *25*, 653.
- (26) Fan, F.-J.; Wu, L.; Gong, M.; Chen, S. Y.; Liu, G. Y.; Yao, H.-B.; Liang, H.-W.; Wang, Y.-X.; Yu, S.-H. *Sci. Rep.* **2012**, *2*, 952.
- (27) Koo, B.; Patel, R. N.; Korgel, B. A. *Chem. Mater.* **2009**, *21*, 1962.
- (28) Marcano, G.; Rincón, C.; López, S. A.; Sánchez Pérez, G.; Herrera-Pérez, J. L.; Mendoza-Alvarez, J. G.; Rodríguez, P. *Solid State Commun.* **2011**, *151*, 84.
- (29) Altosaar, M.; Raudoja, J.; Timmo, K.; Danilson, M.; Grossberg, M.; Krustok, J.; Mellikov, E. *Phys. Status Solidi A* **2008**, *205*, 167.
- (30) Tanaka, T.; Sueishi, T.; Saito, K.; Guo, Q.; Nishio, M.; Yu, K. M.; Walukiewicz, W. *J. Appl. Phys.* **2012**, *111*, 053522.
- (31) Ishii, M.; Shibata, K.; Nozaki, H. *J. Solid State Chem.* **1993**, *105*, 504.